JCTC Journal of Chemical Theory and Computation

Article

pubs.acs.org/JCTC

Scalable Electron Correlation Methods. 2. Parallel PNO-LMP2-F12 with Near Linear Scaling in the Molecular Size

Qianli Ma and Hans-Joachim Werner*

Institut für Theoretische Chemie, Universität Stuttgart, Pfaffenwaldring 55, D-70569 Stuttgart, Baden-Württemberg, Germany

Supporting Information

ABSTRACT: We present an efficient explicitly correlated pair natural orbital local second-order Møller–Plesset perturbation theory (PNO-LMP2-F12) method. The method is an extension of our previously reported PNO-LMP2 approach [Werner et al. *J. Chem. Theory Comput.* **2015**, *11*, 484]. Near linear scaling with the size of molecule is achieved by using domain approximations on both virtual and occupied orbitals, local density fitting (DF), and local resolution of the identity (RI), and by exploiting the sparsity of the local molecular orbitals (LMOs) as well as of projected atomic orbitals (PAOs). All large data structures used in the method are stored in distributed memory using Global Arrays (GAs) to achieve near inverse-linear scaling with the number of processing cores, provided that the GAs can be efficiently and independently accessed from all cores. The effect of the various domain approximations is tested for a wide range of chemical reactions. The PNO-LMP2-F12 reaction energies deviate from the canonical DF-MP2-F12 results by ≤1 kJ mol^{-1} using triple-ζ (VTZ-F12) basis sets and are close to the complete basis set limits. PNO-LMP2-F12 calculations on molecules of chemical interest involving a few thousand basis functions can be performed within an hour or less using a few nodes on a small computer cluster.

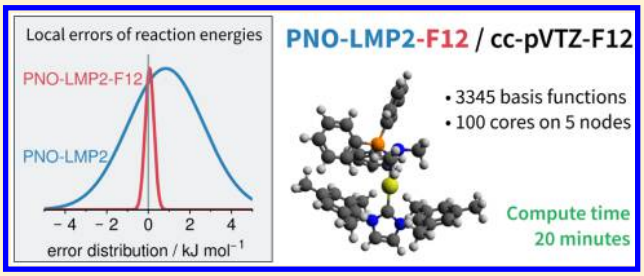

1. INTRODUCTION

The steep scaling of the computational cost with the size of molecules has limited the application of electronic correlation methods to rather small molecules for a long time. Over the years two classes of methods have been developed for tackling this problem: One involves the fragmentation of a molecule into smaller pieces,[1−24] and the other exploits the locality of electron correlation but still explicitly constructs a wave function for the full system.[25−69] The fragmentation-based methods are relatively easy to implement and parallelize, but the fragmentation process can be tricky and unavoidably leads to an enormous amount of redundant calculations, since the fragments must significantly overlap to yield accurate results. Local correlation methods are more efficient but more difficult to implement and parallelize, partly due to the increasing amount of integrals and amplitudes to be stored. The implementation is particularly complicated for modern pair-natural orbital (PNO) methods,[60−74] in which each electron pair uses a different set of virtual orbitals.

Recently, our group has started to construct a new generation of (nearly) scalable local electron correlation methods.[67,68] Here "scalability" means that all computational resources (CPU-time, memory, disk, communication) scale linearly with the molecular size and inversely linearly with the number of computing cores. As a first step, near scalability was demonstrated for a pair natural orbital second-order Møller–Plesset (PNO-LMP2) method[67] (in the following "the preceding paper"). The PNOs were generated in a hierarchical manner using projected atomic orbitals (PAOs) and orbital-specific virtuals (OSVs) in intermediate steps. This treatment, in combination with the local density fitting (LDF) technique, significantly reduced the number of integrals and wave function amplitudes and allowed them to be stored in high-speed memory, distributed over multiple compute nodes. The use of distributed data structures removes the I/O bottlenecks in previously implemented local correlation methods and leads to a PNO-LMP2 method with linear scaling in the molecular size and near-inverse linear scaling in the number of processors.

Including explicitly correlated (F12) terms is essential to the accuracy of local correlation methods, since the F12 contributions have been found to reduce not only basis set incompleteness errors but also the domain errors.[54−58,68] The excellent accuracy of the PNO-LMP2-F12 approach has already been demonstrated in the preceding paper. However, the implementation of the F12 contributions was not yet well parallelized and did not scale linearly with the molecular size. The program relied on large-scale hard-disk I/O for the two-electron integrals and therefore could not efficiently use multiple compute nodes. Also, the method included terms that scale quadratically with the molecular size. These terms arise from the contribution of occupied orbitals in the F12 strong orthogonality projector and slow down the calculation significantly for very large molecules.

In the present work we present a (nearly) scalable F12 implementation. We reduce the scaling and computational cost

Received: September 3, 2015
Published: October 13, 2015

DOI: 10.1021/acs.jctc.5b00843
J. Chem. Theory Comput. 2015, 11, 5291−5304

of F12 calculations by introducing domain approximations for the virtual orbitals (PAOs, PNOs), as well as for the LMOs, which occur in the F12 strong orthogonality projector. Furthermore, local DF and resolution of the identity (RI) approximations are employed, and the sparsities of LMOs and PAOs are exploited to reduce the asymptotic scaling with the molecular size to linear. As in the PNO-LMP2 method, all large data structures are kept in memory and distributed over multiple compute nodes to achieve near inverse-linear scaling in the number of processing cores.

The paper is organized as follows: In Section 2 we briefly outline the basic theory for computing the LMP2-F12 energy correction and describe the local approximations employed, as well as some technical details of our implementation. In Section 3 we demonstrate and analyze the scalability of the PNO-LMP2-F12 method using benchmark calculations on alanine polypeptide helices and some three-dimensional water clusters. The accuracy of the various local approximations is investigated using a test set of reaction energies developed by Friedrich and Hänchen[19] (denoted as FH test set hereafter). A discussion in Section 4 concludes the paper.

2. THEORY AND IMPLEMENTATION

2.1. Explicit Correlation Terms and Domain Selection.

The MP2-F12 theory has been discussed in a number of previous works[44,54,75−81] and will only be outlined briefly in order to introduce the local approximations. For the sake of clarity, we show in Table 1 the abbreviations and index notations for different orbital spaces. In the present work, the occupied molecular orbitals are localized using the intrinsic bond orbital (IBO) method.[82] Core and valence orbitals are localized separately.

Table 1. Index Notation Used for Different Orbital Spaces

orbital space	indices
localized valence molecular orbitals	i, j
localized occupied molecular orbitals	m, n
pair natual orbitals (PNOs)	a^{ij}, b^{ij}
projected atomic orbitals (PAOs)	r, s
density fitting (DF) basis functions	A, B
nonorthogonal RI basis functions	α, β
orthonormal RI functions	$\bar{\alpha}, \bar{\beta}$
atomic orbital (AO) basis functions	μ, ν

In PNO-LMP2-F12 theory the pair correlation functions can be defined as

$$u_{ijp} = \sum_{a,b\in[ij]_{\mathrm{PNO}}} |ab, p\rangle T_{ab}^{ijp} + \hat{Q}_{12}^{ij} F_{12}|ij, p\rangle T_{ij,p} \tag{1}$$

where $p = 1$ or $p = -1$ is for singlet or triplet pairs, respectively, and $|ij,p\rangle = \frac{1}{2}(|ij\rangle + p|ji\rangle)$. T_{ab}^{ijp} are the conventional LMP2 amplitudes for excitations into a domain $[ij]_{\mathrm{PNO}}$ of PNOs, while $T_{ij,p}$ are amplitudes for the explicitly correlated terms. As proposed by Ten-no[76,77] the latter can be determined from the first-order wave function cusp conditions[83,84] and take the values $T_{ij,1} = 1/2$ and $T_{ij,-1} = 1/4$ (independent of ij). F_{12} is a Slater-type geminal[77]

$$F_{12} = -\frac{1}{\gamma} e^{-\gamma r_{12}} \approx -\frac{1}{\gamma} \sum_{i=1}^{6} c_i e^{-\alpha_i r_{12}^2} \tag{2}$$

which is approximated by a linear combination of 6 Gaussians in order to simplify the integral evaluations. Throughout this work, we use the fixed amplitude approximation and set the exponent γ to $1\ a_0^{-1}$. The expansion coefficients and exponents of the Gaussians are taken from ref 80. $\hat{Q}_{12}^{ij}$ is a pair-specific strong orthogonality projector.[54−57] Applying the RI approximation it reads

$$\hat{Q}_{12}^{ij} = 1 - \sum_{a,b\in[ij]_{\mathrm{PNO}}} |ab\rangle\langle ab| + \sum_{m,n\in[ij]_{\mathrm{LMO}}} |mn\rangle\langle mn| - \sum_{m\in[ij]_{\mathrm{LMO}},\bar{\alpha}\in[ij]_{\mathrm{RI}}} (|m\bar{\alpha}\rangle\langle m\bar{\alpha}| + |\bar{\alpha}m\rangle\langle \bar{\alpha}m|) \tag{3}$$

where $[ij]_{\mathrm{PNO}}$, $[ij]_{\mathrm{LMO}}$, and $[ij]_{\mathrm{RI}}$ denote domains of orthonormal PNOs, LMOs, and RI functions for an LMO pair ij, respectively. This form of the projector does not use the complementary auxiliary basis set (CABS) approach[85] and assumes that the RI basis does span the occupied orbital space well. Previous benchmarks have shown that this approximation does not significantly affect the accuracy.[86]

The RI orbitals $\bar{\alpha}$ are orthogonalized for each domain $[ij]_{\mathrm{RI}}$ separately, i.e.,

$$|\bar{\alpha}\rangle = \sum_{\beta\in[ij]_{\mathrm{RI}}} |\beta\rangle [\mathbf{S}_{\mathrm{RI}}^{-1/2}]_{\beta\alpha} \tag{4}$$

The theoretical foundation of using LMO and RI domains in the last two terms of eq 3 is that integrals such as $\langle ij|\hat{F}_{12}|m\alpha\rangle$, which occur in eqs 8 and 9 below, decay exponentially with the distance between the LMOs i and m as well as with the distances between the LMO j and the RI basis functions α (and similarly with i and j exchanged). This means that LMOs m and RI functions α will contribute significantly only if they are spatially close to either i or j. The approximations can cause slight errors in projecting out the contributions of the occupied orbital space, which can lead to small Pauli-principle violating contributions. The errors introduced by these domain approximations on the energy will be demonstrated and discussed in Section 3.

It should be noted that the fixed amplitude approximations with a geminal exponent of $1\ a_0^{-1}$ is not appropriate for treating core and core−valence correlation effects in heavier atoms. This requires either different geminal exponents for core−core, core−valence, and valence−valence pairs, or to optimize the amplitudes of the explicitly correlated terms.[87] These options, which are available in our canonical F12 programs, have not yet been implemented in the local version.

In our current method, the pair-specific external (virtual) space is represented by PNOs, which are generated in a hierarchical treatment using PAO and OSV domains, as described in the preceding paper. All two-electron integrals are evaluated first in the PAO basis and then successively transformed into the OSV and PNO bases. In brief, the domains are determined as follows: Primary PAO domains for each LMO i are first selected using IBO partial charges.[82] The primary PAO domains are then extended by including all PAOs at I_{EXT} shells of neighboring atoms (two atoms are considered to be neighbors if the distance between them is $\leq$1.2 times the sum of their atomic radii), as well as all other atoms within a radius R_{EXT} of any atom in the primary domain. This yields the extended PAO domains $[i]_{\mathrm{PAO}}$. The OSV domains $[i]_{\mathrm{OSV}}$ are selected using an occupation number threshold T_{OSV}, and the pair domains $[ij]_{\mathrm{OSV}}$ are obtained by taking the union of $[i]_{\mathrm{OSV}}$ and $[j]_{\mathrm{OSV}}$. The final PNO domain $[ij]_{\mathrm{PNO}}$ is selected by

DOI: 10.1021/acs.jctc.5b00843
J. Chem. Theory Comput. 2015, 11, 5291−5304

requiring that both an energy criterion T_{PNO} and an occupation number criterion $T_{\mathrm{PNO\_OCC}}$ be fulfilled. The energy criterion ensures that a sufficient number of PNOs is selected for weak pairs. The default values for all parameters will be given in Section 3. More details are described in the preceding paper.

Distant pairs are treated by a simple noniterative multipole approximation[35,36] using OSVs.[62,67] They are not included in the F12 treatment and selected using pair energies estimated by the multipole approximation and a threshold $T_{\mathrm{dist}} = 10^{-6}\ E_h$.

The LMO pair domains $[ij]_{\mathrm{LMO}}$ are taken to be the union of orbital domains $[i]_{\mathrm{LMO}}$ and $[j]_{\mathrm{LMO}}$. These domains determine the range of indices m,n in eq 3 and must include both core and occupied valence orbitals. After some experimentation we found the following domain selection procedure to yield satisfactory results: The valence orbitals $m \in [i]_{\mathrm{LMO}}$ are selected on the basis of the LMP2 pair energies E_{im}^{LMP2} so that $E_{im}^{\mathrm{LMP2}} \geq T_{\mathrm{VAL}}$. Since pair energies are not available for core orbitals, the latter are selected by a connectivity criterion I_{CORE} and a distance criterion R_{CORE}, i.e., the atom at which the core orbital m is localized must be within I_{CORE} bonds or within a distance R_{CORE} from any atom in the primary orbital domain. The RI and DF domains are selected in a similar fashion with criteria I_{RI}, R_{RI} and I_{DF}, R_{DF}, respectively: First, for each RI or DF domain, the atoms which are within the given number of bonds (I_{RI} or I_{DF}) or within the distance criterion (R_{RI} or R_{DF}) of the atoms in the primary orbital domains are selected. Then all RI or DF basis functions at these atoms are included in the corresponding domains.

As in our previous local F12 methods,[54−57] we use the so-called approximation **3*A**,[75,80] in which the extended Brillouin conditions are assumed to be valid and exchange commutator terms $[\hat{k}_1 + \hat{k}_2, F_{12}]$ are neglected. The advantage of this approximation is that all terms are linear in the RI basis, and no RIs involving products of the Fock matrix and the F12 terms arise. Furthermore, the F12 part is noniterative and entirely uncoupled from the conventional LMP2 calculation. In this approximation the F12 correlation energy contribution is given by

$$\Delta E_2^{\mathrm{F12}} = \sum_{i\geq j\in[ij]_{\mathrm{F12}}} (2-\delta_{ij}) \sum_{p=\pm 1} (2-p) T_{ij,p}(2V_{ijp} + T_{ij,p}B_{ijp}) \tag{5}$$

where

$$V_{ijp} = \langle ijp|r_{12}^{-1}\hat{Q}_{12}^{ij}\hat{F}_{12}|ijp\rangle \tag{6}$$

$$B_{ijp} = \langle ijp|[\hat{F}_{12}, \hat{t}_{12}]\hat{Q}_{12}^{ij}\hat{F}_{12}|ijp\rangle \tag{7}$$

and $\hat{t}_{12} = -\frac{1}{2}(\nabla_1^2+\nabla_2^2)$ is the kinetic energy operator for electrons 1 and 2.

The pairs $ij \in [ij]_{\mathrm{F12}}$ for which the F12 correction is computed are selected using LMP2 pair energies and a threshold T_{F12}, i.e., $E_{ij}^{\mathrm{LMP2}} \geq T_{\mathrm{F12}}$. Asymptotically, the number of these pairs scales linearly with molecular size. Through benchmark tests we found a threshold of $T_{\mathrm{F12}} = 10^{-4}\ E_h$ usually gives satisfactory results.

Using the notations $F_{ij,ijp}^{J} = \langle ij|r_{12}^{-1}\hat{F}_{12}|ijp\rangle$, $F_{ij,ijp}^{T} = \langle ij|[\hat{F}_{12}, \hat{t}_{12}]\hat{F}_{12}|ijp\rangle$, $K_{mn}^{ijp} = \langle ijp|r_{12}^{-1}|mn\rangle$, $F_{mn}^{ijp} = \langle ijp|\hat{F}_{12}|mn\rangle$, and $U_{mn}^{ijp} = \langle ijp|[\hat{F}_{12}, \hat{t}_{12}]|mn\rangle$ (and similarly with mn replaced by αm or ab), the quantities in eqs 6 and 7 are computed as

$$V_{ijp} = F_{ij,ijp}^{J} + \sum_{m,n\in[ij]_{\mathrm{LMO}}} F_{mn}^{ijp}K_{mn}^{ijp} - \sum_{m\in[ij]_{\mathrm{LMO}},\alpha\in[ij]_{\mathrm{RI}}} K_{\alpha m}^{ijp}\bar{F}_{\alpha m}^{ijp} - \sum_{a,b\in[ij]_{\mathrm{PNO}}} F_{ab}^{ijp}K_{ab}^{ijp} \tag{8}$$

$$B_{ijp} = F_{ij,ijp}^{T} + \sum_{m,n\in[ij]_{\mathrm{LMO}}} F_{mn}^{ijp}U_{mn}^{ijp} - \sum_{m\in[ij]_{\mathrm{LMO}},\alpha\in[ij]_{\mathrm{RI}}} U_{\alpha m}^{ijp}\bar{F}_{\alpha m}^{ijp} - \sum_{a,b\in[ij]_{\mathrm{PNO}}} F_{ab}^{ijp}U_{ab}^{ijp} \tag{9}$$

Here $\bar{F}_{\alpha m}^{ijp}$ is obtained for each pair separately by solving the linear equations

$$F_{\alpha m}^{ijp} = \sum_{\beta\in[ij]_{\mathrm{RI}}} S_{\alpha\beta}\bar{F}_{\beta m}^{ijp} \tag{10}$$

This accounts for the nonorthogonality of the RI basis functions α with the overlap matrix $S_{\alpha\beta} = \langle\alpha|\beta\rangle$. Since all domain sizes are asymptotically independent of the molecular size, and the number of pairs ij scales linearly with the molecular size, the number of integrals required in computing the F12 correction also scales linearly.

The F12 energy corrections are assembled on the fly while computing the different integral contributions for mn, αm, and ab. For performance reasons, the integrals in eqs 8 and 9 involving PNOs are first evaluated in the PAO basis and then transformed to the PNO space while computing the F12 corrections.

2.2. Local Density Fitting Integral Evaluation and Transformation. Two-electron integral evaluation and transformation is the most time-consuming part of a PNO-LMP2-F12 calculation. In contrast to the PNO-LMP2 calculations, integrals over different kernels and involving RI basis functions as well as atomic orbital (AO) basis functions are needed for the F12 calculations. In this work, we make use of the local density fitting (LDF) method[42,43,50,56,67,88] to evaluate all the two-electron integrals and to perform the integral transformation before fitting and assembly. The required 2-index and 3-index integrals are defined as

$$I_{AB} = \int_{\mathcal{R}_3} d\mathbf{r}_1 \int_{\mathcal{R}_3} d\mathbf{r}_2\, \chi_A(\mathbf{r}_1)\hat{I}\chi_B(\mathbf{r}_2) \tag{11}$$

$$I_{\mu\nu}^{A} = \int_{\mathcal{R}_3} d\mathbf{r}_1 \int_{\mathcal{R}_3} d\mathbf{r}_2\, \chi_A(\mathbf{r}_1)\hat{I}\chi_\mu(\mathbf{r}_2)\chi_\nu(\mathbf{r}_2) \tag{12}$$

The 3-index integrals have to be evaluated for six different kernels $\hat{I}$: $\hat{J} = r_{12}^{-1}$, $\hat{F} = F_{12}$, $\hat{F}^J = \hat{F}_{12}\, r_{12}^{-1}$, $\hat{F}^T = \hat{F}_{12}\,\hat{t}_{12}$, $\hat{X} = [\hat{t}_1, \hat{F}_{12}]$, and $\hat{Y} = [\hat{t}_1, r_{12}^{-1}]$, while the 2-index integrals are only needed for $\hat{J}$ and $\hat{F}$. $\hat{t}_1$ is the kinetic energy operator for electron 1, $\hat{t}_1 = -\frac{1}{2}\nabla_1^2$ and $\hat{t}_{12} = \hat{t}_1 + \hat{t}_2$. The three-index integrals are transformed stepwise into the MO basis

$$I_{\mu i}^{A} = \sum_{\nu} I_{\mu\nu}^{A}L_{\nu i} \tag{13}$$

$$I_{mi}^{A} = \sum_{\mu} I_{\mu i}^{A}L_{\mu m} \tag{14}$$

$$I_{ri}^{A} = \sum_{\mu} I_{\mu i}^{A}P_{\mu r} \tag{15}$$

where $L_{\mu i}$ and $P_{\mu r}$ are LMO and PAO coefficients, respectively. The 3-index integrals $I_{\alpha m}^{A}$ involving RI basis functions χ_α do not

DOI: 10.1021/acs.jctc.5b00843
J. Chem. Theory Comput. 2015, 11, 5291−5304

need a second-half transformation. The transformations are carried out on the fly for blocks of fitting functions A.

To obtain linear scaling in the integral transformations, we exploit the sparsity of the LMO and PAO coefficients by setting small coefficients zero and fitting the approximate LMOs or PAOs to the original ones.[4,67,89] The sparsity check on an LMO vector m is done by setting all coefficients zero if

$$\sum_{\mu \in C} L_{\mu m}^2 \leq T_{\mathrm{LMO}} \tag{16}$$

where the sum runs over all basis functions at a center C. A corresponding check is made for the PAO coefficients $P_{\mu r}$, but in this case the corresponding condition must be fulfilled for all PAOs at the considered center C:

$$\sum_{\mu \in C} P_{\mu r}^2 \leq T_{\mathrm{PAO}}, \quad \forall\, r \in C \tag{17}$$

If the condition is fulfilled, the coefficients $P_{\mu r}$ are set to zero for μ, $r \in C$. By default we use $T_{\mathrm{LMO}} = T_{\mathrm{PAO}} = 10^{-6}$ in the F12 calculations (cf. Section 3.3.1).

The robust fitting approximation[90−92] is used to ensure the accuracy of the integrals, in which the integrals over the $\hat{J}$, $\hat{F}$, $\hat{F}^J$, and $\hat{F}^T$ kernels can be evaluated from, for example

$$F_{\alpha m}^{ij} = \sum_{A \in [i]_{\mathrm{fit}}} d_{i\alpha}^A F_{jm}^A + \sum_{B \in [j]_{\mathrm{fit}}} F_{i\alpha}^B d_{jm}^B - \sum_{A \in [i]_{\mathrm{fit}}, B \in [j]_{\mathrm{fit}}} d_{i\alpha}^A F_{AB} d_{jm}^B \tag{18}$$

while the U integrals take a more complicated form[44,92]

$$U_{\alpha m}^{ij} = \sum_{A \in [i]_{\mathrm{fit}}} (y_{i\alpha}^A F_{jm}^A + d_{i\alpha}^A X_{jm}^A) + \sum_{B \in [j]_{\mathrm{fit}}} (F_{i\alpha}^B y_{jm}^B + X_{i\alpha}^B d_{jm}^B) - \sum_{A \in [i]_{\mathrm{fit}}, B \in [j]_{\mathrm{fit}}} (y_{i\alpha}^A F_{AB} d_{jm}^B + d_{i\alpha}^A F_{AB} y_{jm}^B) \tag{19}$$

where the fitting coefficients d_{ix}^B and y_{ix}^B are obtained by solving the linear equation systems

$$\sum_{B \in [i]_{\mathrm{fit}}} J_{AB} d_{ix}^B = J_{ix}^A, \quad \forall\, A \in [i]_{\mathrm{fit}} \tag{20}$$

$$\sum_{B \in [i]_{\mathrm{fit}}} J_{AB} y_{ix}^B = Y_{ix}^A, \quad \forall\, A \in [i]_{\mathrm{fit}} \tag{21}$$

In the PNO-LMP2 method described in the preceding paper, pair DF domains $A,B \in [ij]_{\mathrm{fit}} = [i]_{\mathrm{fit}} \cup [j]_{\mathrm{fit}}$ were used, so that Coulomb integrals can be computed simply as $J_{\alpha m}^{ij} = \sum_{A \in [ij]_{\mathrm{fit}}} d_{i\alpha}^A J_{jm}^A$. This is robust but requires solving for the fitting coefficients $d_{i\alpha}^A$ by Cholesky decomposition of the J_{AB} matrix for each pair of LMOs ij. This algorithm is less efficient for other types of integrals when the robust fitting formulas in eqs 18 and 19 are required. Instead, orbital fitting domains $A \in [i]_{\mathrm{fit}}$ and $B \in [j]_{\mathrm{fit}}$ are used. The advantage is that in this case the fitting coefficients have to be determined only for each LMO, but the orbital fitting domains have to be larger in order to obtain the same accuracy.[42]

2.3. Integral Screening. The integral screening procedure is similar to that used in the PNO-LMP2 method. We divide the AO and RI basis functions into blocks and assign a bounding sphere for each block. A block of $I_{\mu\nu}^A$ type of integral is only evaluated if the bounding spheres of μ and ν overlap. Otherwise it will be treated as zero in the integral transformation.

The F12-specific integrals all include the $\hat{F}_{12} = -\frac{1}{\gamma} \exp(-\gamma r_{12}^{-1})$ term in the kernel and should decay much faster than the Coulomb integrals as r_{12} increases. This property has not yet been exploited in our integral screening program, in which all integrals are screened on equal footing. Optimizing the F12-specific integral screening may further improve the performance of F12 calculations. Linear scaling in our program is primarily achieved by using the various domain approximations and exploiting the sparsity of LMOs and PAOs. The linear scaling of the integral evaluation and transformation results from the fact that for a given fitting function (or fitting function block) the numbers of contributing LMOs, PAOs, and RI functions become asymptotically independent of the molecular size. The sparsity of the LMO and PAO matrices then limits the ranges of AO indices μ,ν, which are asymptotically independent of the molecular size as well. The integral screening is used only to additionally speed up the calculation, and the error of this screening is negligible in all our tests.

2.4. Technical Aspects and Parallelization. The evaluation and transformation of the 3-index two electron integrals are the most demanding steps in computing the F12 corrections. Once the 3-index integrals are evaluated and transformed, the 4-index integrals and the F12 pair energies can be obtained using simple matrix operations, which is relatively fast. Our parallelization strategy is as follows: We first go through all LMO pairs and make lists of all 3-index integral blocks that are needed to compute the F12 correction. Different lists are needed for the half-transformed and fully transformed integrals. Thus, we know in advance which and how many of these integrals have to be evaluated and transformed. The generation of the lists is parallelized over LMO pairs. The partial lists are finally merged and kept locally on each processor as binary search trees. Storing the lists as hash tables for faster lookup is also possible at the cost of higher memory requirements.

Once the list of necessary 3-index integral blocks is generated, the 3-index integral evaluation and transformation can be performed. This step is dynamically parallelized over blocks of DF functions. First the J and Y integrals are evaluated and transformed on the fly. The transformed integrals are written to global arrays (GAs).[93] In this step the communication involves only nonblocking writing requests to GAs and should not be a bottleneck. Next, the linear eqs 20 and 21 are solved to obtain the fitting coefficients $\mathbf{d}$ and $\mathbf{y}$. This step is dynamically parallelized over LMO labels. If there are more cores than LMOs, the excessive cores stay idle, but the fitting step is very fast and the overall performance is not affected significantly. The density fitting coefficients are also stored in GAs. Since the Y integrals are are not needed in the integral assembly, we remove them from the GA after fitting and before evaluating and transforming other integrals classes.

Finally, the F12 pair energies are calculated. This step is parallelized over pairs. First, the 4-index integrals are assembled, using the 3-index integrals and density fitting coefficients loaded from GA and 2-index integrals J_{AB} and F_{AB} computed on the fly (with a cache to reduce duplicated evaluations) for the required blocks. Finally, the 4-index PAO integrals are transformed to the PNO basis, and the corresponding energy contribution is computed on the fly.

Obviously, the assembly step requires rather massive communication, since all the 3-index integrals have to be read from GAs. If for molecules of different sizes the number of

DOI: 10.1021/acs.jctc.5b00843
J. Chem. Theory Comput. 2015, 11, 5291−5304

cores is proportional to the number of pairs, the amount of data read by each core should be independent of the molecular size, and thus the algorithm should still be scalable (provided that the point-to-point connections between all compute cores are independent of each other). Nevertheless, it is important to minimize the communication load. This is achieved in a 2-fold way: First, the pairs are partitioned so that spatially close LMO pairs are preferably on the same processor. This reduces the communication since the PAO and RI domains of spatially close pairs overlap. The partitioning is done by means of the METIS graph partitioning technique[94] similar to that used in the preceding paper and implies a static parallelization model. Second, a local buffer for each processor is maintained for each type of intermediate quantity to improve the performance. Even though we are not able to measure the communication time directly, we have no indication of a communication bottleneck with an Infiniband network. For example, when the total number of cores stays the same, the elapsed time of a calculation does not increase whether the calculation uses one, two, or more nodes.

An alternative strategy would be to parallelize the whole F12 calculation over pairs and thus avoid communication entirely. Since each pair only requires a finite number of integrals, which is independent of the molecular size, this method should be strictly scalable. However, this would inevitably require redundant integral evaluations and transformations on different processors and would therefore overall be much more expensive. It might be a useful option, however, if the communication bandwidth is slow.

We also exploit the noniterative nature of the **3*A** F12 approximation by dividing the whole computation into two parts, which saves a significant amount of global memory. In the first part we compute the contributions from the first and last terms in the RHS of eqs 8 and 9, for which RI related 3-index integrals are not needed. After that, the PAO related integrals can be freed from GA, and the RI integrals, followed by contributions from other terms, can be computed.

It should be possible to further reduce the required GA space significantly by computing the RI contributions in batches over RI basis functions and store the quantities K_{ai}^{ijp}, F_{ai}^{ijp}, and U_{ai}^{ijp}, which are required in eqs 8−10, in GAs or on disk. We have not implemented this option yet.

One point worth mentioning is that the two-electron Coulomb integrals needed in the PNO-LMP2 and the F12 calculations overlap significantly. Currently we have not combined the integral routines of the two programs or reused the integrals from the PNO-LMP2 calculation in the F12 step. We expect that the integral evaluation technique of the present work would further reduce the cost and memory usage of the already efficient PNO-LMP2 program and also avoid the repeated evaluation of the *J*-integrals in the computation of F12 corrections.

The method is implemented in the development version[95] of the Molpro quantum chemistry package[96] and will be made available for public use in the near future.

3. BENCHMARK CALCULATIONS

3.1. Computation Details. In this section we demonstrate the efficiency of the PNO-LMP2-F12 method through benchmark calculations on alanine polypeptides in the 3_{10}-helical conformation and some some water clusters[20] and test the accuracy for the FH test set of reaction energies.[19] We primarily used the VDZ-F12 and VTZ-F12 basis sets of Peterson et al.[97] that are specially designed for F12 calculations. For a direct comparison of the calculations for the alanine helices with the preceding paper, we used a basis set denoted as aVTZ, which consists of the cc-pVTZ basis sets[98] for H atoms and the aug-cc-pVTZ basis sets[99] for C, N, and O atoms.

Throughout this work DF approximations were carried out for all calculations for the evaluation of two-electron integrals. For optimizing the reference function using density-fitted Hartree−Fock (DF-HF) and for computing the Fock matrix needed in the complementary auxiliary basis set singles correction an aug-cc-pVTZ/JKFIT basis was used. The basis was derived from the cc-pVTZ/JKFIT basis set[100] by adding for each angular momentum another shell of diffuse functions in an even tempered manner. For other integral types the aug-cc-pVTZ/MP2FIT basis set[101] was used. The aug-cc-pVTZ/JKFIT basis set was also employed as RI basis.

Unless otherwise stated, the parameters of local approximations (see Section 2) were kept to our program defaults. Specifically, for the selection of PAO domains we used $I_{EXT} = 2$ and $R_{EXT} = 5a_0$. For OSV and PNO domains, we used $T_{OSV} = 10^{-9}$, $T_{PNO} = 0.997$, and $T_{PNO\_OCC} = 10^{-8}$. The DF and RI domains were selected using the connectivity parameters $I_{DF} = I_{RI} = 3$ and distance parameters $R_{DF} = R_{RI} = 7\ a_0$. The connectivity criteria are included since they take different atomic sizes into account, which lead to longer bond lengths for heavier elements. The distance parameters take into account that atoms may get close even if they are separated by many bonds or in clusters if they are not connected by bonds at all. For pair screening, we used $T_{dist} = 10^{-6}\ E_h$ for removing the distant pairs in PNO-LMP2 calculations, and $T_{F12} = 10^{-4}\ E_h$ for the F12 corrections. The sparsities of PAOs and LMOs were exploited with thresholds of $T_{PAO} = T_{LMO} = 10^{-6}$. These default values are carefully chosen based on extensive benchmark calculations presented in the preceding paper[67] and also later in this section. Again to be consistent with the preceding paper, for the alanine helices we used $T_{LMO} = 10^{-5}$ and selected the DF and RI domains only with the connectivity criteria ($I_{DF} = I_{RI} = 3$). For the largest alanine helix we tested $[(Ala)_{32}]$, these parameters only introduce a <0.002% change in the computed correlation energy compared with the default parameters while reducing the computation cost by ∼25%.

All benchmark calculations were performed on a compute cluster with Xeon E5-2680 v2 @ 2.8 GHz processors. Each node has 2 physical processors with a total of 20 cores and 256 GB of memory. The nodes are connected by an QDR-Infiniband network. All elapsed times reported in this work were obtained using all 20 cores per node. Hyperthreading was not used. We will not distinguish "processors" and "cores" elsewhere in the paper, and only the number of processing cores are considered.

3.2. Alanine Helices. *3.2.1. Analysis of Computation Times.* We first explore the scalability of our PNO-LMP2-F12 method with calculations of the alanine polypeptides $(Ala)_n$ (up to $n = 32$) in the 3_{10} helix confirmation. The alanine helices are not very realistic for real applications but already have rather dense structures with various kinds of intermolecular interactions involved. With the aVTZ basis set, the largest calculation $(Ala)_{32}$ includes 323 atoms, 9674 contracted AO basis functions, 24518 DF basis functions, and 24196 RI basis functions.

Figure 1 demonstrates the scaling of the wall clock times as a function of the number of alanine units. The dotted curve shows the scaling without exploiting the LMO sparsity. When

DOI: 10.1021/acs.jctc.5b00843
J. Chem. Theory Comput. 2015, 11, 5291−5304

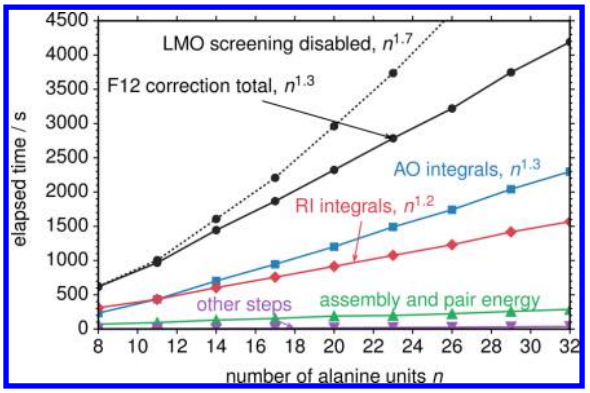

Figure 1. Elapsed times of various steps in computing the F12 corrections in the PNO-LMP2-F12 calculations for alanine polypeptides in the 3_{10}-helical conformation. Computed with 60 cores on 3 nodes. The scaling exponents were obtained from fitting the elapsed times for $(Ala)_{26} - (Ala)_{32}$.

the orbital screening is disabled, the scaling is expected to be cubic for F12 calculations since the 3-index $I^A_{\mu\nu}$-type integrals of various kernels need to be evaluated for all DF and AO basis functions. Integral screening should reduce this to quadratic. In fact, the observed scaling exponent 1.7 is even smaller, due to other lower-scaling steps of the calculations.

With the LMO screening enabled, an overall scaling exponent of 1.3 is achieved, which is slightly larger than the exponent 1.2 observed for the corresponding PNO-LMP2 calculations.[67] As has been shown in the preceding paper, the reason for the slightly nonlinear scaling behavior is that the average number of AOs contributing to each LMO or PAO still grows with the molecular size, even for these rather long chains. This is probably due to the diffuse basis functions and long orthogonalization tails. Exact linear scaling can only be expected if the number of nonzero coefficients per local orbital became independent of the molecular size.

Figure 1 also shows the scaling of the elapsed times for the computationally most demanding steps in the F12 calculations. These include the evaluation and transformation of $I^A_{\mu\nu}$-type integrals of different kernels (denoted as "AO integrals"), the evaluation and transformation of $I^A_{\alpha\mu}$-type integrals (denoted as "RI integrals"), and the assembly of the 4-index integrals and the computation of the F12 pair energies (denoted as "assembly and pair energy"). We see clearly that for all molecules most of the elapsed time is spent on the evaluation and transformation of 3-index integrals. The cost of the integral assembly and other steps, such as making domains or fitting the LMO and PAO coefficients, is quite low.

Considering that the number of RI basis functions is usually 2−3 times larger than the number of AO basis functions, it was initially surprising to see that the evaluation of the AO integrals takes more time than of the RI integrals. However, the AO integrals are further transformed to PAO [I^A_{ri}-type] and LMO [I^A_{mi}-type] integrals before the final assembly, which requires large AO domains since the sparsity of the LMO and PAO coefficients is rather low. For example, the F12 calculation of $(Ala)_{32}$ requires the evaluation of 3687507 blocks of untransformed AO integrals but only 718432 blocks of untransformed RI integrals (here a block includes all basis functions at one atom).

Depending on the molecule and the choice of parameters for the local approximations, a PNO-LMP2-F12 calculation usually takes 3−10 times more computation time than a corresponding PNO-LMP2 calculation. This is the direct consequence of the high cost for evaluating the F12 integrals. We plot in Figure 2

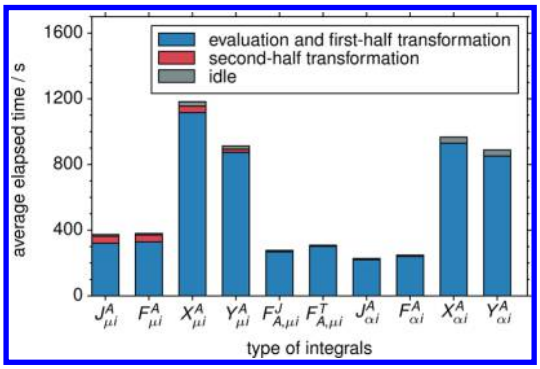

Figure 2. Averaged elapsed times for various 3-index integral evaluations for $(Ala)_{32}$ for each processor. The labels on the x-axis represent the integrals after the first-half transformation. The leftmost 6 integrals are further transformed to I^A_{mi} and I^A_{ri} types. The idle time stands for time spent waiting for other processors to complete the calculation. Computing the density fitting coefficients takes only 25 s in total and is not included in the figure. Computed with 60 cores on 3 nodes.

the average elapsed times for the evaluation and transformation of various 3-index integrals for the F12 calculation of the $(Ala)_{32}$ molecule. The integrals over the commutators $\hat{X} = [\hat{t}_1, \hat{F}_{12}]$ and $\hat{Y} = [\hat{t}_1, r_{12}^{-1}]$ are several times more expensive than the Coulomb integrals, since they involve the kinetic energy operator. The number of Y integrals required is less than that for the X integrals since they are only needed to determine the fitting coefficients $\mathbf{y}$ (see Section 2.2). This is reflected in the relative timings. The time spent on the second-half transformations, i.e., $I^A_{\mu i} \rightarrow I^A_{ri}, I^A_{mi}$, is negligible compared to that spent in the integral evaluation and the first-half transformation. Idle time (waiting for other processors to finish) is also negligible, showing excellent parallel efficiency of the integral routines.

Recently, Kats[102] has proposed a semidirect integral transformation algorithm to obtain the integrals in the PAO basis without using the PAO coefficients directly. This is based on the fact that $\mathbf{P}$ can be expressed in terms of $\mathbf{L}$, i.e., $\mathbf{P} = \mathbf{1} - \mathbf{L}\mathbf{L}^\dagger\mathbf{S}$. This method can potentially improve the performance of the second-half integral transformation. However, since the time for the second-half transformation is almost negligible and the semidirect algorithm of Kats requires complicated bookkeeping procedures, we have not implemented this method in our PNO-LMP2-F12 program.

3.2.2. Memory Usage. Figure 3 shows the actual GA memory usage for the computation of the F12 corrections for $(Ala)_n$ molecules using different F12 pair thresholds T_{F12}. We observe a scaling exponent of 1.1. The GA usage is generally dominated by the RI [$I^A_{\alpha i}$-type] integrals due to the large size of the auxiliary basis sets and RI domains. Using the default threshold $T_{F12} = 10^{-4}\ E_h$, the GA memory usage for $(Ala)_{32}$ amounts to about 160 GB, which is quite moderate for the capacity of modern compute clusters. With smaller values of T_{F12}, the memory usage increases significantly, while the gain in accuracy is small. For the alanine helices, we found the correlation energies obtained with $T_{F12} = 10^{-4}\ E_h$ and $T_{F12} = 10^{-6}\ E_h$ differ by less than 0.002%. Even for the largest molecule we computed here, $(Ala)_{32}$, the absolute difference is only 0.566 mE_h. The GA memory requirement is invariant to the number

DOI: 10.1021/acs.jctc.5b00843
J. Chem. Theory Comput. 2015, 11, 5291−5304

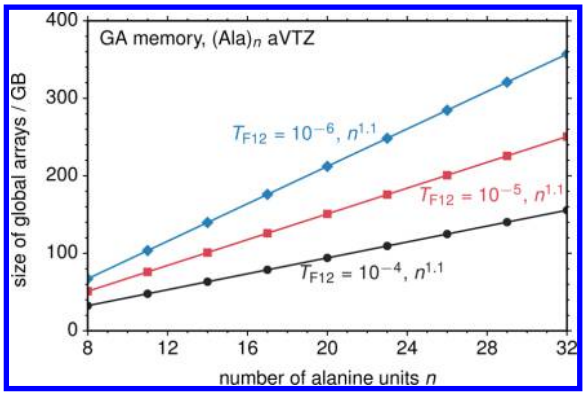

Figure 3. GA memory needed for the PNO-LMP2-F12 calculations as a function of size of the polypeptide chain for $(Ala)_n$. The GA memory usage is invariant to the number of processors used. The local memory requirement for each processor is similar to that for the PNO-LMP2 calculations reported in the preceding paper and is not shown here.

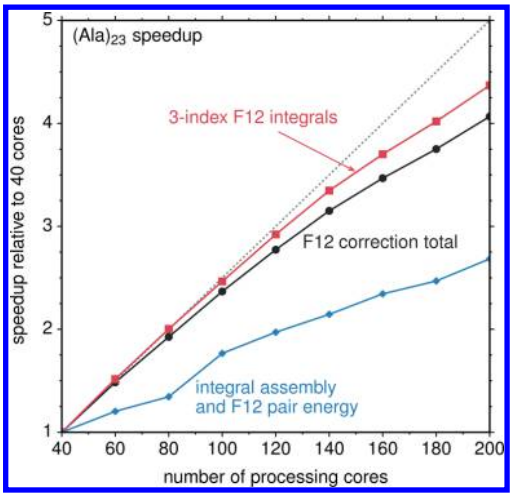

Figure 4. Speedup for the F12 corrections for $(Ala)_{23}$ relative to 40 cores on 2 nodes. The PNO-LMP2 calculation and the F12 correction calculation take 794 and 3985 s, respectively, using 40 cores.

of processors or compute nodes used, and therefore the requirement per node can be reduced by using more nodes.

It should be noted that the local memory per core needed by our program is not yet inversely linear with the molecular size, since some data structures are replicated on all cores. However, in most cases the F12 calculation requires less local memory than the preceding PNO-LMP2 calculation. As already mentioned in the preceding paper, the memory bottleneck in the PNO-LMP2 is due to the replicated storage of some quantities that scale quadratically with molecular size, such as Fock and overlap matrices. Even though all other big data structures scale linearly and are distributed, this can be a bottleneck in large calculations on a small number of compute nodes. For example, the $(Ala)_{32}$ calculation with nearly 10000 basis functions needs about 7 GB of memory per core (in addition to $160/n$ GB GA space, where n is the total number of cores used), and therefore at least 2 or 3 nodes are necessary to run the calculation (depending on the available memory and n).

Further efforts are therefore necessary in order to make the method truly scalable and to be able to perform PNO-LMP2-F12 calculations on molecules beyond a few hundred atoms. As mentioned in Section 2.4, the GA memory usage can potentially be significantly reduced by evaluating and transforming the 3-index RI integrals in batches, while keeping all the $K^{ij}_{\alpha m}$, $F^{ij}_{\alpha m}$, and $U^{ij}_{\alpha m}$ integrals, instead of the 3-index RI integrals, in GAs.

3.2.3. Scaling with the Number of Processors. We show in Figure 4 the speedup with the number of cores with respect to 40 cores for the F12 calculation of the $(Ala)_{23}$ molecule. Overall, the elapsed time of the F12 calculation scales almost linearly with the number of up to ~100 cores. The speedup for the integral evaluation and transformation step is much better than for the assembly step, since the integral evaluation is dynamically parallelized and the communication requests are nonblocking. The integral assembly and F12 pair energy calculation does not parallelize so well, since it uses a static parallelization model and is communication intensive (cf. Section 2.4). Due to the different domain sizes it is quite difficult to achieve a good load balancing, even with the METIS graph partitioning method. In the calculation with 200 cores, 43% of the CPU time is idle due to uneven job partitioning, and the parallel efficiency is only 52%; but overall this step takes a rather short time (cf. Figure 1).

3.3. FH Test Set. To demonstrate the accuracy of the PNO-LMP2-F12 method we present benchmark calculations for a test set of reaction energies developed by Friedrich and Hänchen.[19] The test consists of 104 molecules and 55 reactions of chemical interest. Each reaction involves at least one medium-sized molecule, so that errors introduced by various local approximations can be systematically studied. All calculations have been carried out using the VTZ-F12 basis set. Extensive previous studies[80,86,103−108] have shown that with this basis MP2-F12 calculations typically yield relative energies comparable or better than those obtained with quintuple-ζ basis sets from conventional MP2 calculations. We will therefore not consider basis set incompleteness errors and only focus on errors introduced by the local approximations in the PNO methods. We will first study the convergence of the results with respect to the individual parameters and establish default values. Subsequently, we will present results obtained with this consistent set of parameters.

Detailed results on electronic energies and reaction energies can be found in the Supporting Information.

3.3.1. Effects of Local Approximations. A number of local approximations are made to obtain a linear-scaling algorithm. In the preceding paper extensive test calculations for the approximations used in the PNO-LMP2 program have already been presented. Here we will therefore focus only on new and most relevant approximations in the linear scaling F12 implementation. These include the effect of the LMO screening in the second-half transformation, the LMO domains used in the projector, the DF and RI domains, and the selection of pairs for which the F12 calculation is carried out.

The statistical errors of the correlation and reaction energies of the FH set caused by the LMO screening (cf. Section 2.3) are shown in Figure 5 as a function of the threshold T_{LMO}. The figure shows the deviations relative to calculations without LMO screening. All other parameters are left at their default values. In the preceding paper, we found that a threshold of $T_{LMO} = 10^{-5}$ gives well converged PNO-LMP2 correlation and reaction energies. For F12 calculations the convergence is slower, and a threshold of $T_{LMO} = 10^{-6}$ is needed to obtain an RMSD in reaction energy below 0.1 kJ mol^{-1}. This is likely due to the truncation of LMO coefficients in the second-half integral transformations to obtain I^A_{mi}-type of integrals that are

DOI: 10.1021/acs.jctc.5b00843
J. Chem. Theory Comput. 2015, 11, 5291−5304

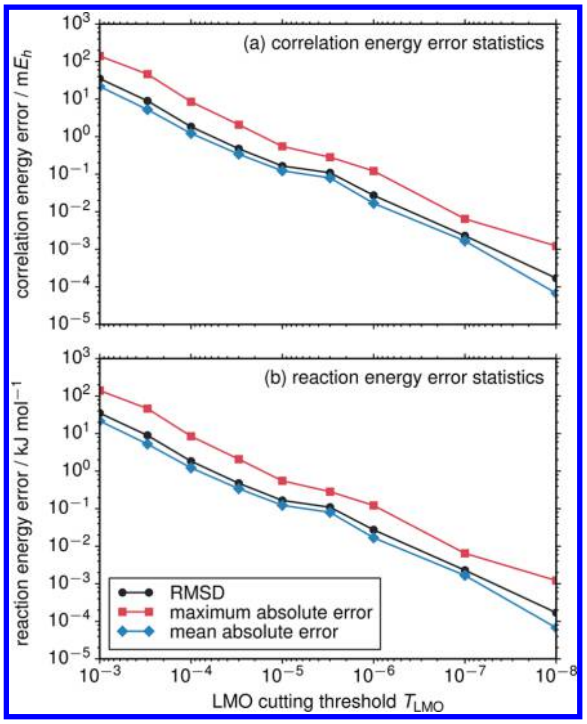

Figure 5. Statistics of errors in PNO-LMP2-F12 (a) correlation and (b) reaction energies introduced by exploiting the sparsity of LMOs as a function of LMO cutting threshold T_{LMO} for the FH test set. The approximate LMOs after cutting are fitted to the original ones. The reference values are obtained without cutting the LMOs. All other parameters for local approximations are kept at the program defaults described in Section 3.1. The VTZ-F12 basis set is used.

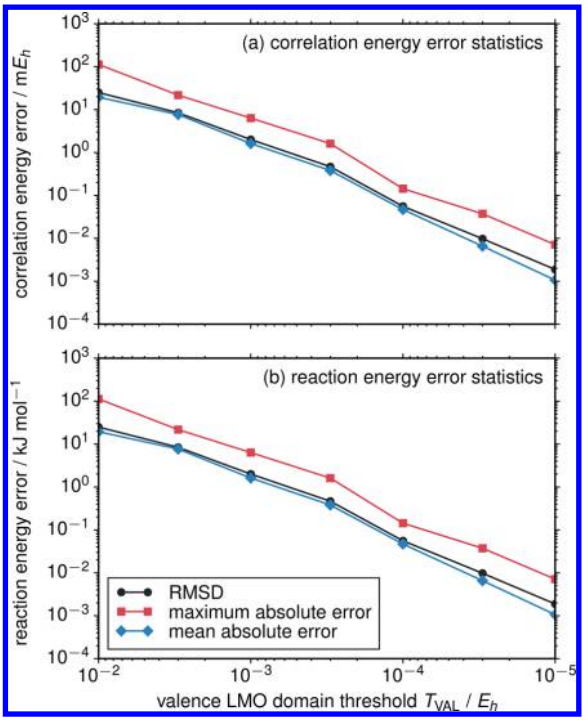

Figure 6. Statistics of errors in PNO-LMP2-F12 (a) correlation and (b) reaction energies introduced by local valence LMO domains as a function of T_{VAL} for the FH test set. The reference values are obtained with full valence LMO domains. All other parameters for local approximations are kept at the program defaults described in Section 3.1. The VTZ-F12 basis set is used.

not required for PNO-LMP2 calculations. The default value of T_{LMO} is thus chosen as 10^{-6}, which is also the default value of truncating PAO coefficients established in the preceding paper.

A similar comparison is made in Figure 6 for the effect of the threshold T_{VAL}, which determines the LMO domains $[ij]_{LMO}$ used in the projector [cf. eqs 3, 8, and 9]. We find that an excellent convergence is achieved at $T_{VAL} = 10^{-4}$ E_h, with the maximum absolute deviations (MAX) and root-mean-square deviations (RMSD) of the correlation energies being 0.14 and 0.05 mE_h, respectively. The corresponding MAX and RMSD for reaction energies are only 0.21 and 0.05 kJ mol^{-1}, respectively. We therefore choose a default value $T_{VAL} = 10^{-4}$ E_h.

The LMO domains also include core orbital domains $[i]_{CORE}$ in addition to the valence orbital domains $[i]_{VAL}$. As mentioned in Section 2.1, the core orbital domains $[i]_{CORE}$ are selected with a combination of distance and connectivity criteria, since they are not correlated in the PNO-LMP2 method and the MP2 pair energies are not available. Since the core orbitals are highly localized at a single atom, the domains can be chosen relatively small. Even with $I_{CORE} = 1$ the errors in the correlation energy introduced by local core orbital domains are less than 2 μE_h for all molecules in the FH set. However, one should be aware that heavy atoms may have more and less localized core orbitals, and the domain errors arising from the core orbital domains can then be slightly larger. For example, for reaction III shown in the Supporting Information, $I_{CORE} = 2$ introduces an error of ~0.2 kJ mol^{-1}. We choose $I_{CORE} = 2$ and $R_{CORE} = 5$ a_0 as our program defaults.

Next, we tested the effect of using local DF and RI domains. The errors of the correlation and reaction energies caused by these approximations are shown in Tables 2 and 3, respectively. In both cases the absolute and relative energies converge smoothly to zero as the domain sizes increase. For most purposes $I_{DF} = I_{RI} = 2$ and $R_{DF} = R_{RI} = 5$ a_0 seem sufficiently accurate, yielding a maximum error of only 0.12 kJ mol^{-1} in the reaction energies. However, the errors might be larger for more extended systems (see, e.g., Section 3.4), and therefore our current defaults are $I_{DF} = I_{RI} = 3$ and $R_{DF} = R_{RI} = 7$ a_0.

Finally, we investigated the effect of selecting the pairs for which the F12 correction is computed using the threshold T_{F12}. The results are nearly identical for pair screening thresholds $T_{F12} = 10^{-4}$ E_h and $T_{F12} = 10^{-6}$ E_h, while $T_{F12} = 10^{-3}$ E_h was found to be insufficient and can lead to errors of up to 2 mE_h in the correlation energies. Therefore, $T_{F12} = 10^{-4}$ E_h is chosen as a default value.

3.3.2. Overall Performance. In this section we will demonstrate the overall accuracy of our method using the default parameters established in the previous section. For this purpose we compare the PNO-LMP2 and PNO-LMP2-F12 calculations with the corresponding canonical DF-MP2 and DF-MP2-F12 calculations, using exactly the same approximations in the F12 parts (Ansatz 3*A with fixed amplitudes).

Figure 7 shows the deviations of the correlation energies and their normal distributions between the local and corresponding canonical methods for 87 larger molecules in the FH set. Using the default parameters for local approximations, the PNO-LMP2 method systematically underestimates the correlation energies, and the domain errors can be as large as 6 mE_h. In the PNO-LMP2-F12 calculations these errors are reduced to less than 1 mE_h.

Figure 8 shows the domain errors and their normal distributions of reaction energies computed with the PNO-LMP2 and PNO-LMP2-F12 methods for all 55 reactions in the

DOI: 10.1021/acs.jctc.5b00843
J. Chem. Theory Comput. 2015, 11, 5291−5304

Table 2. Errors in PNO-LMP2(-F12) Correlation and Reaction Energies Introduced by Local DF Approximations as a Function of I_{DF} and R_{DF} for the FH Test Set[c]

	correlation energy error/mE_h			reaction energy error/kJ mol^{-1}		
	RMSD	MAX[a]	MAD[b]	RMSD	MAX[a]	MAD[b]
PNO-LMP2:						
I_{DF} = 1, R_{DF} = 3 a_0	0.134	0.609	0.105	0.130	0.575	0.091
I_{DF} = 2, R_{DF} = 5 a_0	0.022	0.086	0.017	0.032	0.139	0.020
I_{DF} = 3, R_{DF} = 7 a_0	0.005	0.017	0.003	0.006	0.026	0.004
I_{DF} = 4, R_{DF} = 9 a_0	0.001	0.003	0.001	0.002	0.009	0.001
PNO-LMP2-F12:						
I_{DF} = 1, R_{DF} = 3 a_0	0.042	0.252	0.026	0.081	0.396	0.045
I_{DF} = 2, R_{DF} = 5 a_0	0.008	0.039	0.006	0.018	0.077	0.009
I_{DF} = 3, R_{DF} = 7 a_0	0.002	0.008	0.001	0.004	0.015	0.002
I_{DF} = 4, R_{DF} = 9 a_0	0.000	0.002	0.000	0.001	0.003	0.000

[a]Maximum absolute error. [b]Mean absolute error. [c]The reference values are obtained without local DF. All other parameters for local approximations are kept at the program default described in Section 3.1. Basis set: VTZ-F12.

Table 3. Errors in PNO-LMP2-F12 Correlation and Reaction Energies Introduced by Local RI Approximations as a Function of I_{RI} and R_{RI} for the FH Test Set[c]

	correlation energy error/ mE_h			reaction energy error/ kJ mol^{-1}		
	RMSD	MAX[a]	MAD[b]	RMSD	MAX[a]	MAD[b]
I_{RI} = 1, R_{RI} = 3 a_0	0.283	1.342	0.198	0.338	1.251	0.217
I_{RI} = 2, R_{RI} = 5 a_0	0.021	0.080	0.015	0.031	0.121	0.017
I_{RI} = 3, R_{RI} = 7 a_0	0.004	0.022	0.003	0.006	0.022	0.003
I_{RI} = 4, R_{RI} = 9 a_0	0.001	0.005	0.000	0.002	0.006	0.001

[a]Maximum absolute error. [b]Mean absolute error. [c]The reference values are obtained without local RI. All other parameters for local approximations are kept at the program default described in Section 3.1. Basis set: VTZ-F12.

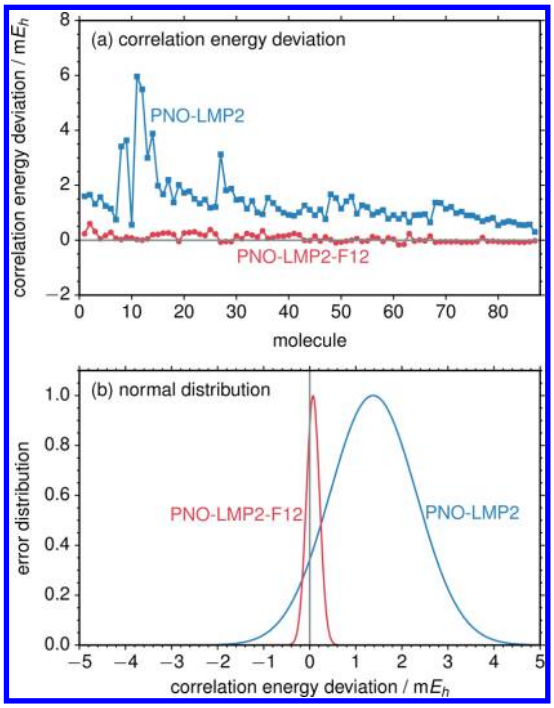

Figure 7. (a) Deviations and (b) normal distributions of correlation energies for the FH test set computed with the PNO-LMP2 (with respect to DF-MP2) method and the PNO-LMP2-F12 (with respect to DF-MP2-F12) method. The PNO calculations were performed with the default parameters for local approximations as described in Section 3.1. Basis set: VTZ-F12.

FH set. Comparing with Figure 7, we find that the domain errors in PNO-LMP2 correlation energies are largely canceled for most of the reactions (1 mH = 2.6255 kJ mol^{-1}). Exceptions include reactions 52 and 53, which are dimerization reactions forming ethylheptamethylcyclobutane and octamethylcyclobutane. In these cases, the reactants are small molecules so that the domain errors in the products cannot cancel out. For all reactions the PNO-LMP2-F12 method gives domain errors well below 1 kJ mol^{-1}.

These tests show that our PNO-LMP2-F12 method only introduces tiny errors in both the correlation and the reaction energies. The method shows excellent efficiency on these midsized molecules as well. The largest molecule in the test set, Me_7Et-cyclobutane, consists of 39 atoms and 1482 AO basis functions. The PNO-LMP2-F12 calculation takes ~5 min using a single node on our cluster. Some additional tests for reactions of larger molecules can be found in the Supporting Information.

3.4. Water Clusters. In this section we further assess the accuracy and scalability of our PNO-LMP2-F12 method with benchmark calculations on six three-dimensional $(H_2O)_{60}$ and $(H_2O)_{100}$ clusters. We have taken the geometries of these clusters (see Figure 9) from ref 20, in which the authors optimized them with molecular mechanics models. The purpose of our calculations is 2-fold: First, we will investigate how the correlation energies of such extended systems converge with the PAO, RI, and DF domain sizes. Second, we will demonstrate that low-order scaling is also achieved for these 3-dimensional systems.

Since the individual molecules are only loosely connected by hydrogen bonds, the connectivity criteria I_{EXT}, I_{DF}, and I_{RI} lead to domains only for each individual H_2O molecule regardless of their values. Therefore, the additional distance criteria R_{EXT}, R_{DF}, and R_{RI} are necessary in these cases. The convergence tests were carried out for structure I of the $(H_2O)_{100}$ cluster and included 8900 basis functions (VTZ-F12 basis). One of the three parameters was varied at a time, while keeping the other two at 9 a_0. We were unable to perform conventional DF-MP2-F12 calculations on these clusters due to the huge hard disk space requirements [>5 TB for $(H_2O)_{60}$, even with the smaller VDZ-F12 basis].

Figure 10 shows the convergence of the PNO-LMP2 (upper panel) and PNO-LMP2-F12 (lower panel) correlation energies

DOI: 10.1021/acs.jctc.5b00843
J. Chem. Theory Comput. 2015, 11, 5291−5304

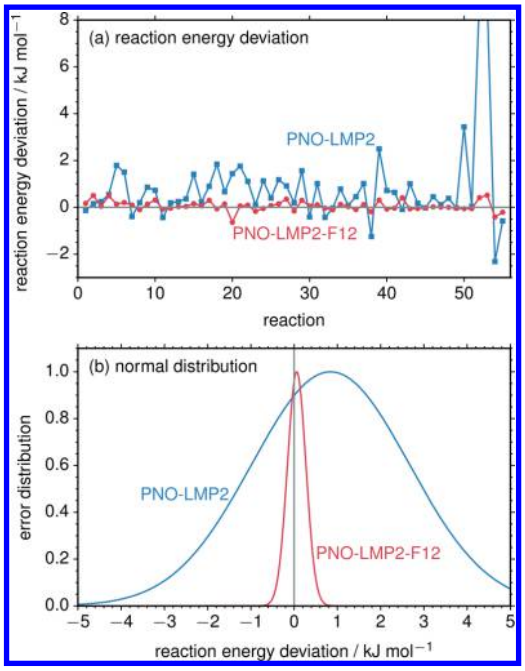

Figure 8. Deviations of reaction energies for the FH test set obtained with the PNO-LMP2 (with respect to DF-MP2) method and the PNO-LMP2-F12 (with respect to DF-MP2-F12) method. The PNO calculations were performed with the default parameters for local approximations as described in Section 3.1. Basis set: VTZ-F12.

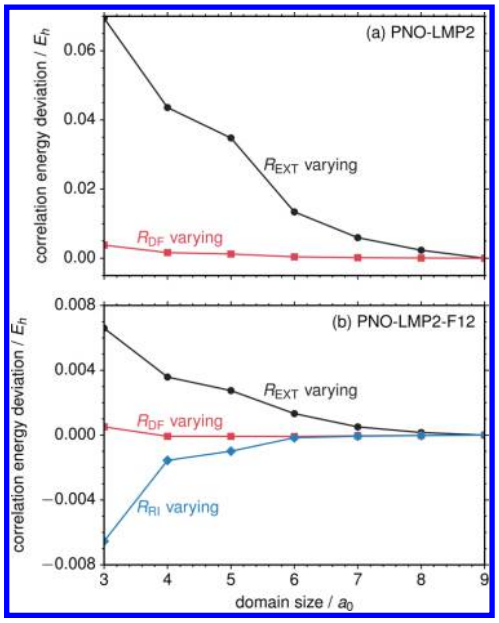

Figure 10. (a) PNO-LMP2 and (b) PNO-LMP2-F12 correlation energy deviations as functions of the parameters R_{EXT}, R_{DF}, and R_{RI} for the $(H_2O)_{100}$ (I) cluster. The reference correlation energies (−27.881011 E_h for PNO-LMP2 and −30.735352 E_h for PNO-LMP2-F12) are obtained with $R_{EXT} = R_{DF} = R_{RI} = 9\ a_0$. One parameter is varied at a time, while the other two are kept at 9 a_0. The VTZ-F12 basis set is used.

as a function of the domain sizes. For this cluster, the convergence of the PNO-LMP2 correlation energy with the PAO domain size (determined by R_{EXT}) is very slow; the correlation energies obtained with $R_{EXT} = 8\ a_0$ and 9 a_0 still differ by 1.3 mE_h. We believe that this effect is mainly caused by basis set superposition errors (BSSE), which are largely removed in local calculations with small PAO domains[31,109,110] and reintroduced with increasing PAO domain sizes. This effect is reduced by 1 order of magnitude in the PNO-LMP2-F12 calculations (note the different scales in the two panels of Figure 10), which supports the assumption that BSSE is the reason for the slow convergence with R_{EXT}.

The error introduced by local DF is negligible, even with a relatively small domain size of $R_{DF} = 5\ a_0$. The RI domain sizes are more critical. It is generally observed that small RI basis sets lead to an overestimation of the F12 energies, and this is also the case if the RI-domains are too small. In these cases, the strong-orthogonality projector cannot fully remove contributions from occupied orbitals, and the remaining Pauli-principle violating contributions will lower the energy. As a result, there may be a fortuitous error cancellation if small PAO and RI domains are used in combination.

Other local approximations in our method, such as the F12 pair selection and LMO domains, are based on pair energies rather than distances and are expected to be less sensitive to the structures and sizes of the clusters. We have therefore not

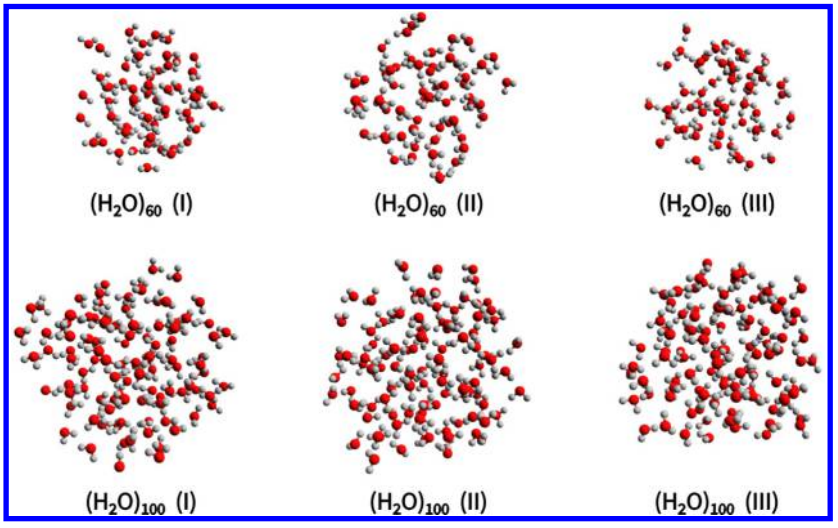

Figure 9. Geometries of water clusters studied in this work.

DOI: 10.1021/acs.jctc.5b00843
J. Chem. Theory Comput. 2015, 11, 5291−5304

pursued further convergence tests of these parameters for the water clusters.

Figure 11 shows the dependence of the elapsed times for the PNO-LMP2 calculation of $(H_2O)_{100}$ (dashed lines) and the

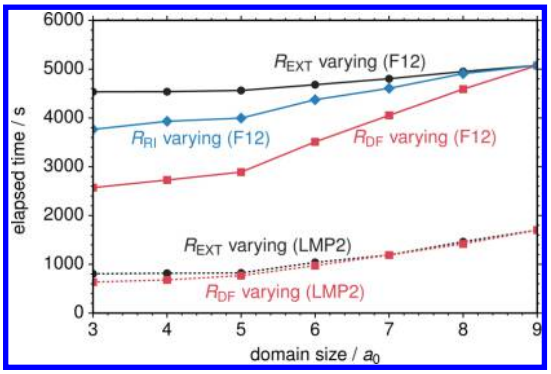

Figure 11. Elapsed time as a function of domain sizes for the PNO-LMP2-F12 calculations of the $(H_2O)_{100}$ molecule (structure I). Elapsed times for F12 corrections are shown in solid lines, and the times for PNO-LMP2 calculations are shown in dotted lines. The results obtained from varying the PAO, DF, and RI domain sizes are shown. One parameter is varied at a time, while the other two are kept at 9 a_0. All calculations are performed using 100 cores on 5 nodes. The VTZ-F12 basis set is used.

F12 contribution (full lines) as functions of R_{EXT}, R_{DF}, and R_{RI}, again varying one parameter at a time and leaving the others at 9 a_0. The strongest effect is seen for the parameter R_{DF}, in particular for the F12 part. The DF domain sizes also strongly affect the memory requirements, and therefore R_{DF} should be kept as small as possible. To be on the safe side, the default values were set to $I_{DF} = 3$, $R_{DF} = 7$ a_0, and these values have also been used for most benchmark calculations in the present paper. However, it appears that $I_{DF} = 2$, $R_{DF} = 5$ a_0 would be sufficient.

Total elapsed times for the PNO-LMP2-F12 calculations for the 6 clusters are shown in Table 4, using three different combinations of domain sizes. Using the default values a PNO-LMP2-F12 calculation for $(H_2O)_{100}$ with VTZ-F12 basis takes about 80 min and with VDZ-F12 basis about 40 min, using 80 cores on 4 nodes. Scaling exponents can be obtained formally by comparing the times for $(H_2O)_{60}$ and $(H_2O)_{100}$, and this has been done by comparing structures $(H_2O)_{60}$ (x) with $(H_2O)_{100}$ (x), where x = I, II, or III. It should be pointed out that there is no relation between the structures which have been assigned numbers I, II, or III, and therefore comparing, e.g., $(H_2O)_{60}$ (I) with $(H_2O)_{100}$ (I) and not with $(H_2O)_{100}$ (II) or (III) is entirely arbitrary. The scaling exponents obtained with both basis sets and all choices of domain sizes are quite similar. The most surprising result is the large difference in the elapsed times for the three $(H_2O)_{60}$ clusters, which strongly affects the scaling exponents, depending on which clusters are compared. For example, comparing cluster structures I yields scaling exponents of about 1.1−1.2, while for clusters II and III they are around 2.2−2.3.

Closer inspection shows that even though the primary domains are the same in all cases, comprising just the centers and corresponding basis functions for individual water molecules, the extended domain sizes differ significantly. In particular, for $(H_2O)_{60}$ structure I has much larger extended domains than structures II or III. This indicates that structure I is more dense than the others, even though this cannot be easily recognized from the pictures in Figure 9. One could argue that the different extended domain sizes are an artifact of using real space distance parameters, but the number of pairs treated in the LMP2 after removing all distant pairs that have estimated pair energies below $T_{dist} = 10^{-6}$ E_h show the same trends. The same is also true for the number of F12 pairs, which are selected using the energy criterion $T_{F12} = 10^{-4}$ E_h. For $(H_2O)_{60}$ also the LMO sparsities are much larger for structures II or III than for structure I. These results demonstrate that the computational resources depend not only on the size of molecular clusters but also sensitively on their 3-dimensional structure. The averaged lengths of PAO and LMO vectors for $(H_2O)_{100}$ are significantly larger than those for $(H_2O)_{60}$, which shows that the asymptotic behavior is not yet achieved for these clusters. From the current results it is therefore not possible to conclude whether the scaling is truly linear. In order to obtain meaningful scaling factors, one would need to construct artificial structures that are consistent for different cluster sizes.

4. CONCLUSIONS

In this work, we have reported an efficient PNO-LMP2-F12 implementation and extensive benchmarks to establish its accuracy and efficiency. The method scales nearly linear with molecular size and nearly inverse-linear with the number of processors for large molecules, provided that the GAs can be efficiently and independently accessed from all compute cores.

The accuracy of the local approximations is controlled by a few parameters, and we have demonstrated through a comprehensive test set and a few larger chemical systems (see the Supporting Information) that the errors of reaction energies due to the various local approximations are well below ∼1 kJ mol^{-1}, using a default set of parameters and the VTZ-F12 basis set.

Our PNO-LMP2-F12 method is efficiently implemented by eliminating redundant integral evaluations and making use of the sparsity of the local molecular orbitals (LMOs, PAOs), as well as by exploiting domain and pair approximations. With the present implementation we were able to carry out PNO-LMP2-F12 calculations of three-dimensional molecules and molecular clusters with up to nearly 10000 basis functions in ∼1 h of elapsed time, using 60−100 processing cores (3−5 compute nodes). Machines of this size are available to many groups in quantum chemistry, and we believe that it is more important to develop efficient programs for such clusters than for massively parallel supercomputers.

We have tested our program using up to 200 processing cores and have observed satisfactory parallel efficiency. Since the disk I/O is completely avoided, and cost of communication is relatively insignificant, our method can potentially also be employed on massively parallel systems to allow the study of very large molecules. For that purpose, we will need to further reduce the memory requirements by avoiding the replicated and dense storage of LMO, PAO, overlap, and Fock matrices as well as some other data structures such as integral block lists. Also implementation of a hierarchical parallel structure with a shared-memory model could further improve the efficiency by reducing the communication cost through buffering data in shared memory.

The errors caused by the local approximations in our methods are significantly smaller than the intrinsic error of the MP2 model, but the F12 correction obtained by the PNO-LMP2-F12 method can also be used in combination with more

DOI: 10.1021/acs.jctc.5b00843
J. Chem. Theory Comput. 2015, 11, 5291−5304

Table 4. Elapsed Times and Other Relevent Information of the PNO-LMP2-F12 Calculations for Water Clusters[g]

	VDZ-F12 basis set			VTZ-F12 basis set		
structure	I	II	III	I	II	III
Number of Nondistant Pairs[a]						
$(H_2O)_{60}$	9030 (1608)	6900 (1208)	6916 (1229)	9164 (1720)	7023 (1280)	7043 (1314)
$(H_2O)_{100}$	13446 (2269)	13657 (2306)	13964 (2380)	13689 (2408)	13898 (2464)	14119 (2543)
Average PAO Domain Size[b]						
$(H_2O)_{60}$	333.0	234.4	241.5	611.4	434.6	444.7
$(H_2O)_{100}$	268.7	274.1	282.3	498.1	508.0	523.5
Average PNO Domain Size[b]						
$(H_2O)_{60}$	24.9	23.4	23.7	36.4	34.5	35.0
$(H_2O)_{100}$	23.7	23.7	24.0	34.6	34.7	35.1
Average Valence LMO Vector Length[c]						
$(H_2O)_{60}$	1846.1	1452.9	1429.1	3934.0	3218.8	3162.8
$(H_2O)_{100}$	2157.0	2202.3	2208.3	5008.2	5137.4	5169.2
ratio[d]	1.17	1.52	1.55	1.27	1.60	1.63
Average PAO Vector Length[e]						
$(H_2O)_{60}$	2329.5	1920.8	1869.7	4019.9	3295.7	3237.1
$(H_2O)_{100}$	2857.2	2908.9	2919.8	4927.1	5060.7	5106.7
ratio[d]	1.23	1.51	1.56	1.23	1.54	1.58
Elapsed Time Using R_{EXT} = 3 a_0, R_{DF} = 5 a_0, and R_{RI} = 5 a_0[f]						
$(H_2O)_{60}$	680 (588)	398 (346)	398 (346)	1486 (1236)	883 (752)	880 (756)
$(H_2O)_{100}$	1229 (1060)	1280 (1112)	1316 (1124)	2753 (2341)	2852 (2442)	2899 (2462)
scaling exponent	1.16 (1.15)	2.29 (2.29)	2.34 (2.31)	1.21 (1.25)	2.30 (2.31)	2.33 (2.31)
Elapsed Time Using R_{EXT} = 5 a_0, R_{DF} = 7 a_0, and R_{RI} = 7 a_0[f]						
$(H_2O)_{60}$	1287 (1102)	763 (670)	767 (679)	2489 (2075)	1500 (1288)	1516 (1316)
$(H_2O)_{100}$	2314 (1999)	2429 (2082)	2478 (2149)	4744 (4029)	4904 (4162)	5074 (4295)
scaling exponent	1.15 (1.17)	2.27 (2.22)	2.30 (2.26)	1.26 (1.30)	2.32 (2.30)	2.36 (2.32)
Elapsed Time Using R_{EXT} = 7 a_0, R_{DF} = 7 a_0, and R_{RI} = 7 a_0[f]						
$(H_2O)_{60}$	1437 (1162)	808 (692)	825 (703)	2979 (2290)	1625 (1344)	1702 (1387)
$(H_2O)_{100}$	2457 (2050)	2550 (2146)	2662 (2222)	5161 (4150)	5464 (4336)	5667 (4513)
scaling exponent	1.05 (1.11)	2.25 (2.22)	2.29 (2.25)	1.08 (1.16)	2.37 (2.29)	2.35 (2.31)

[a]MP2 pairs with $T_{dist} = 10^{-6}$ E_h and F12 pairs (in parentheses) with $T_{F12} = 10^{-4}$ E_h. [b]Selected using R_{EXT} = 7, $T_{OSV} = 10^{-9}$, T_{PNO} = 0.997, and $T_{PNO\_OCC} = 10^{-8}$. [c]LMOs truncated with $T_{LMO} = 10^{-6}$. [d]$(H_2O)_{100}$ against $(H_2O)_{60}$. Asymptotically this should be 1. [e]PAOs truncated with $T_{PAO} = 10^{-6}$. [f]Connectivity criteria for domain selection are not used. Total elapsed times for PNO-LMP2-F12 and elapsed times for the F12 correction (in parentheses) are shown. [g]Computed with 80 cores on 4 nodes. Comparing the $(H_2O)_{60}$ and $(H_2O)_{100}$ clusters with the same structure label I, II, or III is completely arbitrary.

sophisticated correlation methods such as PNO-LCCSD(T). A full local implementation of CCSD-F12 models such as CCSD-F12x[86,105] (x = a,b) requires the evaluation of F12 coupling terms in the CCSD equations. This has already been achieved previously in our group for closed-shell[57] and open-shell[111] PAO-LCCSD-F12x methods, but it turned out that the coupling terms are very difficult and expensive to evaluate for large molecules. However, previous benchmarks[105] have shown that complete neglect of these couplings is a surprisingly good approximation. This means that the F12 correction can be simply added to the PNO-LCCSD energy, or, vice versa, a CCSD correction can be added to the PNO-LMP2-F12 energy. This is very much in the spirit of composite correlation models such as G2 or G3 theories. For example, in a recent study of reaction III shown in the Supporting Information, a PNO-LCCD correction of −56.2 kJ mol^{-1} was added to the PNO-LMP2-F12 reaction energy of 250.1 kJ mol^{-1}, yielding a result of 193.9 kJ mol^{-1}, in good agreement with a gas-phase experimental value of 196.5 ± 11.2 kJ mol^{-1} (zero-point corrections were included). A low-order scaling, parallel PNO-LCCSD(T)-F12 program is currently under development in our group.

■ ASSOCIATED CONTENT

Supporting Information

The Supporting Information is available free of charge on the ACS Publications website at DOI: 10.1021/acs.jctc.5b00843.

Detailed tables of correlation energies and reaction energies for the FH test set, as well as results for some reactions of large molecules (PDF)

■ AUTHOR INFORMATION

Corresponding Author

*E-mail: werner@theochem.uni-stuttgart.de.

Notes

The authors declare no competing financial interest.

■ ACKNOWLEDGMENTS

This work is supported by the European Research Council (ERC) Advanced Grant 320723 (ASES).

■ REFERENCES

(1) Fedorov, D. G.; Kitaura, K. *J. Chem. Phys.* **2005**, *123*, 134103.
(2) Friedrich, J.; Hanrath, M.; Dolg, M. *J. Chem. Phys.* **2007**, *126*, 154110.
(3) Friedrich, J.; Dolg, M. *J. Chem. Phys.* **2008**, *129*, 244105.

DOI: 10.1021/acs.jctc.5b00843
J. Chem. Theory Comput. 2015, 11, 5291−5304

(4) Li, W.; Piecuch, P.; Gour, J. R.; Li, S. *J. Chem. Phys.* **2009**, *131*, 114109.
(5) Gordon, M. S.; Mullin, J. M.; Pruitt, S. R.; Roskop, L. B.; Slipchenko, L. V.; Boatz, J. A. *J. Phys. Chem. B* **2009**, *113*, 9646−9663.
(6) Friedrich, J.; Dolg, M. *J. Chem. Theory Comput.* **2009**, *5*, 287−294.
(7) Friedrich, J.; Coriani, S.; Helgaker, T.; Dolg, M. *J. Chem. Phys.* **2009**, *131*, 154102.
(8) Ziółkowski, M.; Jansík, B.; Kjærgaard, T.; Jørgensen, P. *J. Chem. Phys.* **2010**, *133*, 014107.
(9) Li, W.; Piecuch, P. *J. Phys. Chem. A* **2010**, *114*, 8644−8657.
(10) Li, W.; Piecuch, P. *J. Phys. Chem. A* **2010**, *114*, 6721−6727.
(11) Fedorov, A.; Couzijn, E. P. A.; Nagornova, N. S.; Boyarkin, O. V.; Rizzo, T. R.; Chen, P. *J. Am. Chem. Soc.* **2010**, *132*, 13789−13798.
(12) Kristensen, K.; Ziółkowski, M.; Jansík, B.; Kjærgaard, T.; Jørgensen, P. *J. Chem. Theory Comput.* **2011**, *7*, 1677−1694.
(13) Li, W.; Guo, Y.; Li, S. *Phys. Chem. Chem. Phys.* **2012**, *14*, 7854−7862.
(14) Kristensen, K.; Jørgensen, P.; Jansik, B.; Kjærgaard, T.; Reine, S. *J. Chem. Phys.* **2012**, *137*, 114102.
(15) Høyvik, I.-M.; Kristensen, K.; Jansik, B.; Jørgensen, P. *J. Chem. Phys.* **2012**, *136*, 014105.
(16) Gordon, M. S.; Fedorov, D. G.; Pruitt, S. R.; Slipchenko, L. V. *Chem. Rev.* **2012**, *112*, 632−672.
(17) Li, W. *J. Chem. Phys.* **2013**, *138*, 014106.
(18) Kristensen, K.; Kjærgaard, T.; Høyvik, I.-M.; Ettenhuber, P.; Jørgensen, P.; Jansik, B.; Reine, S.; Jakowski, J. *Mol. Phys.* **2013**, *111*, 1196−1210.
(19) Friedrich, J.; Hänchen, J. *J. Chem. Theory Comput.* **2013**, *9*, 5381−5394.
(20) Saha, A.; Raghavachari, K. *J. Chem. Theory Comput.* **2014**, *10*, 58−67.
(21) Yoshikawa, T.; Nakai, H. *J. Comput. Chem.* **2015**, *36*, 164−170.
(22) Li, W.; Chen, C.; Zhao, D.; Li, S. *Int. J. Quantum Chem.* **2015**, *115*, 641−646.
(23) Findlater, A. D.; Zahariev, F.; Gordon, M. S. *J. Phys. Chem. A* **2015**, *119*, 3587−3593.
(24) Eriksen, J. J.; Baudin, P.; Ettenhuber, P.; Kristensen, K.; Kjærgaard, T.; Jørgensen, P. *J. Chem. Theory Comput.* **2015**, *11*, 2984−2993.
(25) Pulay, P. *Chem. Phys. Lett.* **1983**, *100*, 151−154.
(26) Sæbø, S.; Pulay, P. *Chem. Phys. Lett.* **1985**, *113*, 13−18.
(27) Pulay, P.; Saebø, S. *Theor. Chim. Acta* **1986**, *69*, 357−368.
(28) Saebø, S.; Pulay, P. *J. Chem. Phys.* **1987**, *86*, 914−922.
(29) Saebo, S.; Pulay, P. *J. Chem. Phys.* **1988**, *88*, 1884−1890.
(30) Hampel, C.; Werner, H.-J. *J. Chem. Phys.* **1996**, *104*, 6286−6297.
(31) Schütz, M.; Rauhut, G.; Werner, H.-J. *J. Phys. Chem. A* **1998**, *102*, 5997−6003.
(32) Maslen, P. E.; Head-Gordon, M. *Chem. Phys. Lett.* **1998**, *283*, 102−108.
(33) Maslen, P. E.; Head-Gordon, M. *J. Chem. Phys.* **1998**, *109*, 7093−7099.
(34) Schütz, M.; Hetzer, G.; Werner, H.-J. *J. Chem. Phys.* **1999**, *111*, 5691−5705.
(35) Hetzer, G.; Pulay, P.; Werner, H.-J. *Chem. Phys. Lett.* **1998**, *290*, 143−149.
(36) Hetzer, G.; Schütz, M.; Stoll, H.; Werner, H.-J. *J. Chem. Phys.* **2000**, *113*, 9443−9455.
(37) Schütz, M.; Werner, H.-J. *Chem. Phys. Lett.* **2000**, *318*, 370−378.
(38) Schütz, M. *J. Chem. Phys.* **2000**, *113*, 9986.
(39) Schütz, M.; Werner, H.-J. *J. Chem. Phys.* **2001**, *114*, 661−681.
(40) Schütz, M. *Phys. Chem. Chem. Phys.* **2002**, *4*, 3941−3947.
(41) Schütz, M. *J. Chem. Phys.* **2002**, *116*, 8772−8785.
(42) Werner, H.-J.; Manby, F. R.; Knowles, P. J. *J. Chem. Phys.* **2003**, *118*, 8149−8160.
(43) Schütz, M.; Manby, F. R. *Phys. Chem. Chem. Phys.* **2003**, *5*, 3349−3358.
(44) Manby, F. R.; Werner, H.-J.; Adler, T. B.; May, A. J. *J. Chem. Phys.* **2006**, *124*, 094103.
(45) Auer, A. A.; Nooijen, M. *J. Chem. Phys.* **2006**, *125*, 024104.
(46) Hrenar, T.; Rauhut, G.; Werner, H.-J. *J. Phys. Chem. A* **2006**, *110*, 2060−2064.
(47) Mata, R.; Werner, H.-J. *J. Chem. Phys.* **2006**, *125*, 184110.
(48) Mata, R. A.; Werner, H.-J. *Mol. Phys.* **2007**, *105*, 2753−2761.
(49) Mata, R.; Werner, H.-J.; Schütz, M. *J. Chem. Phys.* **2008**, *128*, 144106.
(50) Werner, H.-J.; Schütz, M. *J. Chem. Phys.* **2011**, *135*, 144116.
(51) Schütz, M.; Yang, J.; Chan, G. K.-L.; Manby, F. R.; Werner, H.-J. *J. Chem. Phys.* **2013**, *138*, 054109.
(52) Chwee, T. S.; Szilva, A. B.; Lindh, R.; Carter, E. A. *J. Chem. Phys.* **2008**, *128*, 224106.
(53) Doser, B.; Lambrecht, D. S.; Kussmann, J.; Ochsenfeld, C. *J. Chem. Phys.* **2009**, *130*, 064107.
(54) Werner, H.-J. *J. Chem. Phys.* **2008**, *129*, 101103.
(55) Adler, T. B.; Werner, H.-J. *J. Chem. Phys.* **2009**, *130*, 241101.
(56) Adler, T. B.; Werner, H.-J.; Manby, F. R. *J. Chem. Phys.* **2009**, *130*, 054106.
(57) Adler, T. B.; Werner, H.-J. *J. Chem. Phys.* **2011**, *135*, 144117.
(58) Krause, C.; Werner, H.-J. *Phys. Chem. Chem. Phys.* **2012**, *14*, 7591−7604.
(59) Maschio, L. *J. Chem. Theory Comput.* **2011**, *7*, 2818−2830.
(60) Neese, F.; Wennmohs, F.; Hansen, A. *J. Chem. Phys.* **2009**, *130*, 114108.
(61) Neese, F.; Hansen, A.; Liakos, D. G. *J. Chem. Phys.* **2009**, *131*, 064103.
(62) Riplinger, C.; Neese, F. *J. Chem. Phys.* **2013**, *138*, 034106.
(63) Demel, O.; Pittner, J.; Neese, F. *J. Chem. Theory Comput.* **2015**, *11*, 3104−3114.
(64) Tew, D. P.; Helmich, B.; Hättig, C. *J. Chem. Phys.* **2011**, *135*, 074107.
(65) Hättig, C.; Tew, D. P.; Helmich, B. *J. Chem. Phys.* **2012**, *136*, 204105.
(66) Schmitz, G.; Helmich, B.; Hättig, C. *Mol. Phys.* **2013**, *111*, 2463−2476.
(67) Werner, H.-J.; Knizia, G.; Krause, C.; Schwilk, M.; Dornbach, M. *J. Chem. Theory Comput.* **2015**, *11*, 484−507.
(68) Schwilk, M.; Usvyat, D.; Werner, H.-J. *J. Chem. Phys.* **2015**, *142*, 121102.
(69) Köppl, C.; Werner, H.-J. *J. Chem. Phys.* **2015**, *142*, 164108.
(70) Edmiston, C.; Krauss, M. *J. Chem. Phys.* **1965**, *42*, 1119.
(71) Meyer, W. *Int. J. Quantum Chem.* **1971**, *5*, 341.
(72) Meyer, W. *J. Chem. Phys.* **1973**, *58*, 1017.
(73) Ahlrichs, R.; Driessler, F.; Lischka, H.; Staemmler, V.; Kutzelnigg, W. *J. Chem. Phys.* **1975**, *62*, 1235.
(74) Staemmler, V.; Jaquet, R. *Theor. Chim. Acta* **1981**, *59*, 487.
(75) Klopper, W.; Samson, C. C. M. *J. Chem. Phys.* **2002**, *116*, 6397−6410.
(76) Ten-no, S. *J. Chem. Phys.* **2004**, *121*, 117−129.
(77) Ten-no, S. *Chem. Phys. Lett.* **2004**, *398*, 56−61.
(78) May, A. J.; Manby, F. R. *J. Chem. Phys.* **2004**, *121*, 4479−4485.
(79) Werner, H.-J.; Manby, F. R. *J. Chem. Phys.* **2006**, *124*, 054114.
(80) Werner, H.-J.; Adler, T. B.; Manby, F. R. *J. Chem. Phys.* **2007**, *126*, 164102.
(81) Ten-no, S.; Noga, J. *WIREs J. Comput. Mol. Sci.* **2012**, *2*, 114−125.
(82) Knizia, G. *J. Chem. Theory Comput.* **2013**, *9*, 4834−4843.
(83) Kato, T. *Commun. Pure Appl. Math.* **1957**, *10*, 151−177.
(84) Pack, R. T.; Brown, W. B. *J. Chem. Phys.* **1966**, *45*, 556−559.
(85) Valeev, E. F. *Chem. Phys. Lett.* **2004**, *395*, 190−195.
(86) Adler, T. B.; Knizia, G.; Werner, H.-J. *J. Chem. Phys.* **2007**, *127*, 221106.
(87) Werner, H.-J.; Knizia, G.; Manby, F. R. *Mol. Phys.* **2011**, *109*, 407−417.
(88) Polly, R.; Werner, H.-J.; Manby, F. R.; Knowles, P. J. *Mol. Phys.* **2004**, *102*, 2311−2321.
(89) Boughton, J. W.; Pulay, P. *J. Comput. Chem.* **1993**, *14*, 736−740.
(90) Dunlap, B. I. *Int. J. Quantum Chem.* **1997**, *64*, 193−203.
(91) Dunlap, B. I. *Phys. Chem. Chem. Phys.* **2000**, *2*, 2113−2116.

DOI: 10.1021/acs.jctc.5b00843
J. Chem. Theory Comput. 2015, 11, 5291−5304

(92) Manby, F. R. *J. Chem. Phys.* **2003**, *119*, 4607−4613.
(93) Nieplocha, J.; Palmer, B.; Tipparaju, V.; Krishnan, M.; Trease, H.; Apra, E. *Int. J. High Perform C* **2006**, *20*, 203−231.
(94) Karypis, G.; Kumar, V. *SIAM J. Sci. Comput.* **1998**, *20*, 359−392.
(95) Werner, H.-J.; Knowles, P. J.; Knizia, G.; Manby, F. R.; Schütz, M. et al. MOLPRO, development version, 2015.1, a package of ab initio programs. 2015. See http://www.molpro.net (accessed Oct 1, 2015).
(96) Werner, H.-J.; Knowles, P. J.; Knizia, G.; Manby, F. R.; Schütz, M. *WIREs Comput. Mol. Sci.* **2012**, *2*, 242−253.
(97) Peterson, K. A.; Adler, T. B.; Werner, H.-J. *J. Chem. Phys.* **2008**, *128*, 084102.
(98) Dunning, T. H. *J. Chem. Phys.* **1989**, *90*, 1007−1023.
(99) Kendall, R. A.; Dunning, T. H.; Harrison, R. J. *J. Chem. Phys.* **1992**, *96*, 6796−6806.
(100) Weigend, F. *Phys. Chem. Chem. Phys.* **2002**, *4*, 4285−4291.
(101) Weigend, F.; Köhn, A.; Hättig, C. *J. Chem. Phys.* **2002**, *116*, 3175−3183.
(102) Kats, D. *J. Chem. Phys.* **2014**, *141*, 244101.
(103) Tew, D. P.; Klopper, W.; Neiss, C.; Hättig, C. *Phys. Chem. Chem. Phys.* **2007**, *9*, 1921−1930.
(104) Knizia, G.; Werner, H.-J. *J. Chem. Phys.* **2008**, *128*, 154103.
(105) Knizia, G.; Adler, T. B.; Werner, H.-J. *J. Chem. Phys.* **2009**, *130*, 054104.
(106) Tew, D. P.; Hättig, C.; Bachorz, R. A.; Klopper, W. In *Recent Progress in Coupled Cluster Methods*; Čársky, P., Paldus, J., Pittner, J., Eds.; Springer: Dordrecht, Heidelberg, London, NY, 2010; pp 535−572.
(107) Werner, H.-J.; Adler, T. B.; Knizia, G.; Manby, F. R. In *Recent Progress in Coupled Cluster Methods*; Čársky, P., Paldus, J., Pittner, J., Eds.; Springer: Dordrecht, Heidelberg, London, NY, 2010; pp 573−619.
(108) Werner, H.-J.; Knizia, G.; Adler, T. B.; Marchetti, O. *Z. Phys. Chem.* **2010**, *224*, 493.
(109) Saebø, S.; Tong, W.; Pulay, P. *J. Chem. Phys.* **1993**, *98*, 2170−2175.
(110) Runeberg, N.; Schütz, M.; Werner, H.-J. *J. Chem. Phys.* **1999**, *110*, 7210.
(111) Agapito, F.; Liu, Y.; Werner, H.-J. To be published.

DOI: 10.1021/acs.jctc.5b00843
J. Chem. Theory Comput. 2015, 11, 5291−5304